Biochem. J. (2008) **414**, 471–484 (Printed in Great Britain) doi:10.1042/BJ20080149

online data multimedia

The secretion inhibitor Exo2 perturbs trafficking of Shiga toxin between endosomes and the *trans*-Golgi network

Robert A. SPOONER*[1], Peter WATSON*[1,2], Daniel C. SMITH*[1,3], Frédéric BOAL†, Mohammed AMESSOU‡, Ludger JOHANNES‡, Guy J. CLARKSON§, J. Michael LORD*, David J. STEPHENS†[4] and Lynne M. ROBERTS*[4]

*Department of Biological Sciences, University of Warwick, Gibbet Hill Road, Coventry CV4 7AL, U.K., †Department of Biochemistry, University of Bristol, School of Medical Sciences, University Walk, Bristol BS8 1TD, U.K., ‡Institut Curie, Centre de Recherche, Laboratoire Trafic, Signalisation, et Ciblage Intracellulaires, 26 rue d'Ulm, 75248 Paris Cedex 05, France, and CNRS (Centre National de la Recherche Scientifique) UMR144, France, and §Department of Chemistry, University of Warwick, Gibbet Hill Road, Coventry CV4 7AL, U.K.

The small-molecule inhibitor Exo2 {4-hydroxy-3-methoxy-(5,6,7,8-tetrahydrol[1]benzothieno[2,3-*d*]pyrimidin-4-yl)hydrazone benzaldehyde} has been reported to disrupt the Golgi apparatus completely and to stimulate Golgi–ER (endoplasmic reticulum) fusion in mammalian cells, akin to the well-characterized fungal toxin BFA (brefeldin A). It has also been reported that Exo2 does not affect the integrity of the TGN (*trans*-Golgi network), or the direct retrograde trafficking of the glycolipid-binding cholera toxin from the TGN to the ER lumen. We have examined the effects of BFA and Exo2, and found that both compounds are indistinguishable in their inhibition of anterograde transport and that both reagents significantly disrupt the morphology of the TGN in HeLa and in BS-C-1 cells. However, Exo2, unlike BFA, does not induce tubulation and merging of the TGN and endosomal compartments. Furthermore, and in contrast with its effects on cholera toxin, Exo2 significantly perturbs the delivery of Shiga toxin to the ER. Together, these results suggest that the likely target(s) of Exo2 operate at the level of the TGN, the Golgi and a subset of early endosomes, and thus Exo2 provides a more selective tool than BFA for examining membrane trafficking in mammalian cells.

Key words: brefeldin A (BFA), Exo2, Golgi, membrane traffic, secretory pathway, Shiga toxin (STx).

INTRODUCTION

Although much of our knowledge of the secretory pathway comes from genetic or biochemical experiments [1,2], small-molecule inhibitors have also proven to be extremely useful tools for studying this pathway. Perhaps the best example is the fungal isoprenoid metabolite BFA (brefeldin A), which causes rapid dissociation of COPI (coatomer protein I) coats from Golgi membranes [3,4] and consequent tubulation and subsequent merging of Golgi membranes with those of the ER (endoplasmic reticulum) [5,6]. BFA also induces very rapid and dramatic tubulation of EEs (early endosomes) and causes a redistribution of the TGN (*trans*-Golgi network) and endosomes, including microtubule-dependent fusion of the TGN and EEs [7–9]. Many of the effects of BFA are mediated by its inhibition of GEFs (guanine-nucleotide-exchange factors) that act on the small GTPases of the ARF (ADP-ribosylation factor) family [10–12]. BFA acts as an interfacial inhibitor [13–15], binding and stabilizing an abortive complex of ARF-GEF–ARF1–GDP, thereby preventing GDP/GTP exchange and inhibiting ARF1 activation [16].

Previous chemical genetics approaches have identified further inhibitors of secretory pathway function that appear to cause similar effects to those of BFA. Two inhibitors, termed Exo1 [2-(4-fluorobenzoylamino)-benzoic acid methyl ester] [17] and Exo2 {4-hydroxy-3-methoxy-(5,6,7,8-tetrahydrol[1]benzothieno-[2,3-*d*]pyrimidin-4-yl)hydrazone benzaldehyde} [18], show little structural similarity to BFA but, importantly, they demonstrate some near-identical effects in a number of assays. Although the targets of Exo1 and Exo2 remain unknown, Exo1 has been shown not to interfere with GEF-stimulated GDP/GTP exchange on ARF; it somehow interferes with the ARF-dependent GTP hydrolysis step [17]. Nothing is known about the precise target(s) of Exo2, but, as with Exo1, a description of the phenotype promoted by this inhibitor will help to guide and focus future studies into finding this protein. It has already been reported that Exo2 blocks secretory cargo exit from the ER and disrupts the Golgi apparatus, but does not affect the morphology of the TGN [18]. Since the trafficking of the glycolipid-binding CTx (cholera toxin) from the cell surface to the ER remained unaffected in Exo2-treated cells, as did continued sulfation of a modified CTx subunit that was believed to occur during passage through the TGN, an alternative pathway for the direct transport of CTx from the TGN to the ER has been proposed [18]. These results are significant in that they define a retrograde-trafficking pathway based on the continued integrity of the TGN in the presence of Exo2. This leads to the possibility of exploiting the different effects of BFA and Exo2 to examine such a pathway more fully.

In the present paper, using a different set of organelle markers and the well-characterized lipid-binding STx (Shiga toxin), we have examined the effects of BFA and Exo2 in mammalian

Abbreviations used: ARF, ADP-ribosylation factor; BFA, brefeldin A; COPI, coatomer protein I; CTx, cholera toxin; Cy3, indocarbocyanine; DMEM, Dulbecco's modified Eagle's medium; EE, early endosome; EEA1, early endosome antigen 1; EGFP, enhanced green fluorescent protein; ER, endoplasmic reticulum; ERGIC, ER–Golgi intermediate compartment; Exo2, 4-hydroxy-3-methoxy-(5,6,7,8-tetrahydrol[1]benzothieno[2,3-*d*]pyrimidin-4-yl)hydrazone benzaldehyde; FCS, foetal calf serum; GalT, galactosyltransferase; Gb3, globotriaosylceramide; GEF, guanine-nucleotide-exchange factor; GM130, *cis*-Golgi matrix protein of 130 kDa; NAGFP, EGFP fused to the Golgi retention signal of *N*-acetylglucosaminyltransferase I; STx, Shiga toxin; STxB, STx B chain; STxBsulf, STxB bearing an accessible sulfation motif; TfR, transferrin receptor; TGN, *trans*-Golgi network; TPST, tyrosylprotein sulfotransferase; tsO45-G, temperature-sensitive vesicular-stomatitis virus-G mutant; YFP, yellow fluorescent protein.

[1] These authors contributed equally to this work.

[2] Present address: School of Biosciences, Cardiff University, Museum Avenue, Cardiff CF10 3US, U.K.

[3] Present address: Cobra Biomanufacturing Plc, Stephenson Building, The Science Park, Keele ST5 5SP, U.K.

[4] Correspondence may be addressed to either of these authors (lynne.roberts@warwick.ac.uk or david.stephens@bristol.ac.uk).

cells. Using a combination of fixed- and live-cell imaging and functional examination of retrograde-trafficking pathways, we confirm that these two compounds have indistinguishable effects on anterograde transport from the ER-to-Golgi and on the Golgi. However, unlike BFA, Exo2 does not induce tubulation of endosomal compartments. Moreover, and in contrast with results published previously [18], we find that Exo2 disrupts the morphology of the TGN, and that the retrograde transport of STx is severely compromised in two toxin-sensitive cell lines. These results reveal subtle but important differences in the effects of BFA and Exo2 on endomembrane organization and function, and on the trafficking of different lipid-binding toxins.

EXPERIMENTAL

Materials

For immunofluorescence studies, HeLa (A.T.C.C. CCL-2) cells were grown on glass-bottomed dishes (MatTek) or 22 mm-diameter coverslips in DMEM (Dulbecco's modified Eagle's medium; Life Technologies)/FCS (foetal calf serum) medium supplemented with 10 % (v/v) FCS and 1 % L-glutamine. Rabbit polyclonal anti-giantin antibody was from Covance. Mouse monoclonal anti-GM130 (*cis*-Golgi matrix protein of 130 kDa), mouse monoclonal anti-EEA1 (early endosome antigen 1) and mouse monoclonal anti-calnexin antibodies were from BD Transduction Laboratories. Sheep polyclonal anti-TGN46 antibody was from AbD Serotec and mouse monoclonal anti-ERGIC (ER–Golgi intermediate compartment)-53 antibody was from Alexis Biochemicals. Mouse monoclonal anti-GalT (galactosyltransferase) antibody was from CellMAb. Monoclonal mouse anti-CD63 antibody (Biogenesis) was a gift from Dr Harry Mellor (Department of Biochemistry, University of Bristol, Bristol, U.K.). Alexa Fluor® dye-labelled secondary antibodies (anti-rabbit, anti-mouse and anti-sheep IgG antibodies; all highly cross-adsorbed), Alexa Fluor® 568-labelled transferrin, mouse monoclonal anti-golgin-97 antibody (clone CDF4), mouse monoclonal anti-TfR (transferrin receptor) antibody and LysoTracker Red were from Invitrogen.

Cytotoxicity measurements

Cells were seeded at 2×10^4 cells per well in 96-well plates in DMEM/FCS (HeLa and Vero cells), GMEM (Glasgow minimal essential medium)/10 % (v/v) FCS (BS-C-1 cells; A.T.C.C. CCL-26) or 1:1 (v/v) DMEM/Ham's F12 medium containing 5 % (v/v) FCS (T84 cells), grown overnight at 37 °C, washed with PBS and were then incubated for 30 min at 37 °C in the appropriate growth medium containing trafficking inhibitor (50 μM Exo2 and 0.05 % DMSO vehicle) or vehicle only (10 $\mu g \cdot ml^{-1}$ BFA and 0.5 % ethanol vehicle). The cells were then incubated with graded dilutions of STx in the relevant growth medium containing trafficking inhibitor or vehicle as appropriate for 1, 2 or 4 h at 37 °C. Cytotoxicity was measured as the ability of cells to incorporate [^{35}S]methionine into acid-precipitable material after toxin treatment, using an assay published previously [19]. IC_{50} values (in $ng \cdot ml^{-1}$) were determined using a median-effect plot [20].

Immunofluorescence and live cell-imaging

Live and fixed cells were imaged using wide-field microscopy as described previously [20a]. Where indicated, cells were treated with nocodazole (5 μM; Sigma), BFA (10 μM; Sigma) or with an equal volume of DMSO (vehicle only) for 1 h at 37 °C in the appropriate culture medium. For immunofluorescence, cells were fixed with methanol at − 20 °C for 4 min, blocked using PBS containing 3 % (w/v) BSA and incubated with primary antibodies [anti-EEA1 antibody (1:500 dilution), anti-CD63 antibody (1:1000 dilution), anti-giantin antibody (1:2000 dilution), anti-ERGIC-53 antibody (1:100 dilution), anti-Sec31A antibody (1:100 dilution), anti-golgin-97 antibody (1:500 dilution), anti-TGN46 antibody (1:500 dilution), anti-calnexin antibody (1:100 dilution), anti-GalT antibody (1:500 dilution), anti-TfR antibody (1:500 dilution) and anti-COPI antibody (1:100 dilution)] for 1 h. LysoTracker Red was used following the manufacturer's instructions. For staining of EEA1, cells were fixed with 3.5 % (w/v) paraformaldehyde in PBS for 15 min at room temperature (18–25 °C) and permeabilized by incubation with 0.1 % Triton X-100 in PBS for 5 min at room temperature. For CD63 staining, paraformaldehyde-fixed cells were permeabilized with 0.5 % saponin in PBS for 5 min at room temperature, with all subsequent steps performed in the presence of 0.1 % saponin. Alexa Fluor® 488-, Alexa Fluor® 568- or Alexa Fluor® 647-conjugated antibodies (anti-rabbit, anti-mouse and anti-sheep IgG antibodies; 1:800 dilution) and Cy3 (indocarbocyanine)-labelled antibody (1:500 dilution; Jackson ImmunoResearch) were used as secondary antibodies. Alexa Fluor® 568-conjugated transferrin was diluted in growth medium and added to cells at a final concentration of 10 $\mu g \cdot ml^{-1}$. Images and time-lapse sequences were acquired 5 min after incubation with Alexa Fluor® 568-conjugated transferrin. Wide-field images were acquired as described previously [21]. Confocal sections were acquired using a Leica TCS SP2 AOBS scanning-confocal microscope with illumination from the 543 nm line of a HeNe laser (for Alexa Fluor® 568-conjugated transferrin) and 405 nm diode laser [for DAPI (4′,6-diamidino-2-phenylindole)]. A pinhole size of 1 Airy disk and a pixel size of 100 nm were used, and images were acquired using the linear range of the detector. All images were processed using Photoshop CS (Adobe), ImageJ [NIH (National Institutes of Health)] and QuickTime Pro (Apple). Montages were generated using Adobe Illustrator CS (Adobe). Movies were compiled in QuickTime Pro using 'Photo JPEG' compression.

Sulfation analysis

Sulfation analysis was preformed as described previously [22]. Briefly, HeLa cells seeded at 2×10^5 cells per well in 12-well plates were grown overnight at 37 °C, starved of sulfate for 90 min, with the last 30 min of this starvation period performed in the presence of DMSO or 50 μM Exo2 in DMSO and, after washing twice with PBS, STxBsulf [STxB (STx B chain) bearing an accessible sulfation motif] was added and the cells were incubated on ice for 30 min. After washing twice with PBS, $^{35}SO_4$ (300 $\mu Ci \cdot ml^{-1}$; Amersham Biosciences) in sulfate-free medium containing DMSO or Exo2/DMSO as appropriate was added, and STxBsulf was immunoprecipitated from detergent-soluble extracts after 0, 20, 40, 60, 120, 180 and 240 min of incubation at 37 °C. In order to determine endogenous sulfation, sulfated proteins in supernatants obtained after quantitative STxB immunoprecipitation were precipitated with 10 % (v/v) trichloroacetic acid, retained on GF/C glass-fibre filtres (Whatman) and scintillation counted.

Molecular cloning of TPST (tyrosylprotein sulfotransferase)–EGFP (enhanced green fluorescent protein)

The TPST1 and TPST2 sequences were obtained from human ESTs (expressed sequence tags) from the RZPD (Deutsches Ressourcenzentrum für Genomforschung, Berlin, Germany; GenBank® accession numbers NM_003596 and AF061254

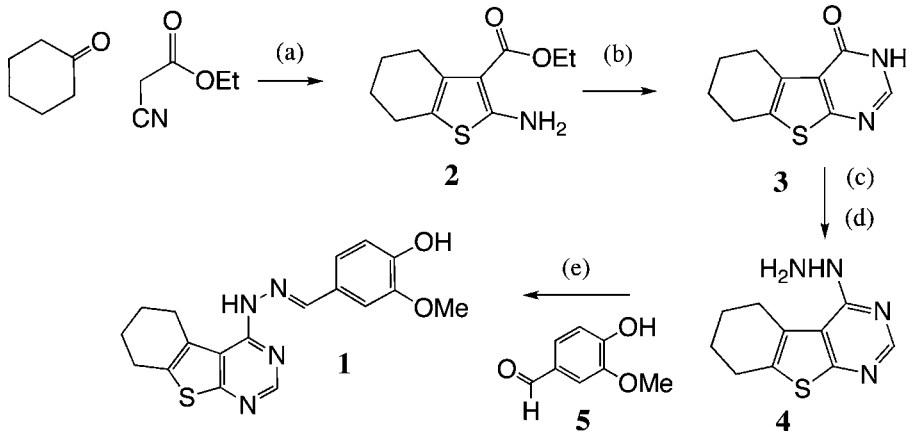

Figure 1 Synthesis of Exo2

The central thienopyrimidone unit (3) was constructed by condensation of cyanoamide with cyclohexanone in the presence of sulfur [27] to give aminothiophene (2) and cyclization with formamide [28–30]. Chloride formation [31] and displacement gave the hydrazine (4) [32]. Condensation with vanillin (5) yielded Exo2 (1). The reactions in the scheme are: (a) piperidine/sulfur (b) formamide/reflux, (c) phosphorus chloride oxide/dimethylaniline, (d) hydrazine hydrate in methanol, (e) vanillin in methanol.

respectively). TPST1–EGFP and TPST2–EGFP were obtained by PCR using the following primers: plus strand, 5′-GGGGCTCGAGATGGTTGGAAAGCTGAAG-3′, and minus strand, 5′-GGGGCTGCAGCTCCACTTGCTCAGTC-3′ for TPST1; and plus strand, 5′-GGGGCTCGAGATGCGCCTGTCGGTGC-3′, and minus strand, 5′-GGGGCTGCAGCGAGCTTCCTAAGTGG-3′ for TPST2 (XhoI and PstI, restriction sites are underlined). PCR products were purified and ligated into the pGEM-T-Easy vector (Promega) following the manufacturer's instructions. Positive clones were digested with XhoI and PstI, and the fragments obtained were inserted in the corresponding sites of pEGFP-N1 (Clontech). All constructs were verified by double-strand DNA sequencing (MWG Biotech, Ebersburg, Germany). Two differences to the published sequence of TPST2 were identified (276C>T and 1002T>C, relative to the start codon), but neither of which affect the predicted protein sequence.

RESULTS

Exo2 treatment strongly protects cells against STx challenge

CTx and STx bind cell surface ganglioside GM1 and Gb3 (globotriaosylceramide) respectively and are delivered via EEs and the TGN to the ER lumen, in association with detergent-resistant microdomains, in a manner that is not dependent on either KDEL receptors or COPI-transport intermediates [23–26]. When human intestinal T84 cells were treated with Exo2, an inhibitor of secretion isolated from the DIVERSetE chemical library (Chembridge, San Diego, CA, U.S.A.) [17], they remained fully sensitive to CTx, leading to a model whereby ER-trafficking lipid-binding retrograde cargoes bypass the Golgi stack, moving directly from the TGN to the ER [18]. To test this model further, we therefore examined the effects of Exo2 on the uptake of STx.

We first manufactured Exo2 as shown in Figure 1. Briefly, the central thienopyrimidone unit (3) was set up by condensation of the cyanoamide with cyclohexanone in the presence of sulfur [27] to give aminothiophene (2) and cyclization with formamide [28–30]. Chloride formation [31] and displacement gave hydrazine (4) [32]. Condensation with vanillin (5) yielded Exo2 (1). Stock solutions were made at 100 mM in DMSO and stored in aliquots at −20 °C.

Upon arrival into the ER, the enzymatic A1 chain of STx retro-translocates across the ER membrane, entering the cytosol, where it inactivates ribosomes and halts protein synthesis [33]. HeLa cells, pre-treated for 30 min with vehicle alone (0.05 % DMSO) or with 50 μM Exo2, were incubated with dilutions of STx in growth medium containing DMSO or Exo2/DMSO as appropriate for various times, and the remaining ability to synthesize protein was measured (Figure 2A). Exo2 rendered cells strongly resistant to STx challenge, but the level of resistance varied with toxin exposure times (Figure 2C). Following short toxin treatments (1 h), Exo2-treated cells were ∼150-fold more resistant to STx than vehicle-treated cells that had been exposed to the same doses of toxin. However, following 4 h exposure to toxin, Exo2-treated cells were only ∼12-fold more resistant than vehicle-treated cells.

STx is activated by furin, which nicks the intact STxA polypeptide to generate a processed and activated A1 chain [34]. Since an Exo2-mediated block in anterograde transport might alter the steady-state distribution of furin, the strong protective effects observed may simply reflect an alteration in the trafficking or replenishment rate of this facilitating enzyme. To preclude this possibility, we pre-activated the toxin with trypsin (Figure 2B), which nicks the A chain at its furin-sensitive site [34], and found this made little difference to the protection observed (Figure 2C), showing that the resistances observed are not caused by delayed or incomplete processing of the toxin.

As a comparison, cells were pre-treated with 10 $\mu g \cdot ml^{-1}$ BFA (dissolved in ethanol) or the vehicle solvent alone (0.5 % ethanol), and then treated with dilutions of STx in growth medium containing ethanol or ethanol/BFA as appropriate (Figure 2A). BFA treatment resulted in protective effects against STx that were too large to measure at the concentrations and times used.

In African green-monkey-kidney-derived Vero and BS-C-1 cells, rates of CTx internalization and TGN and ER arrival were unchanged following Exo2 treatment [18]. This contrasts with the observations of the present paper when STx is applied to HeLa cells. Therefore to check for a cell-type-dependent effect, we tested the sensitivity of these kidney-derived cell lines to STx when treated with Exo2. For Vero cells, which have a similar sensitivity to STx as HeLa cells, the protective effect of Exo2 was very large, approx. 1200-fold for a 4 h toxin challenge

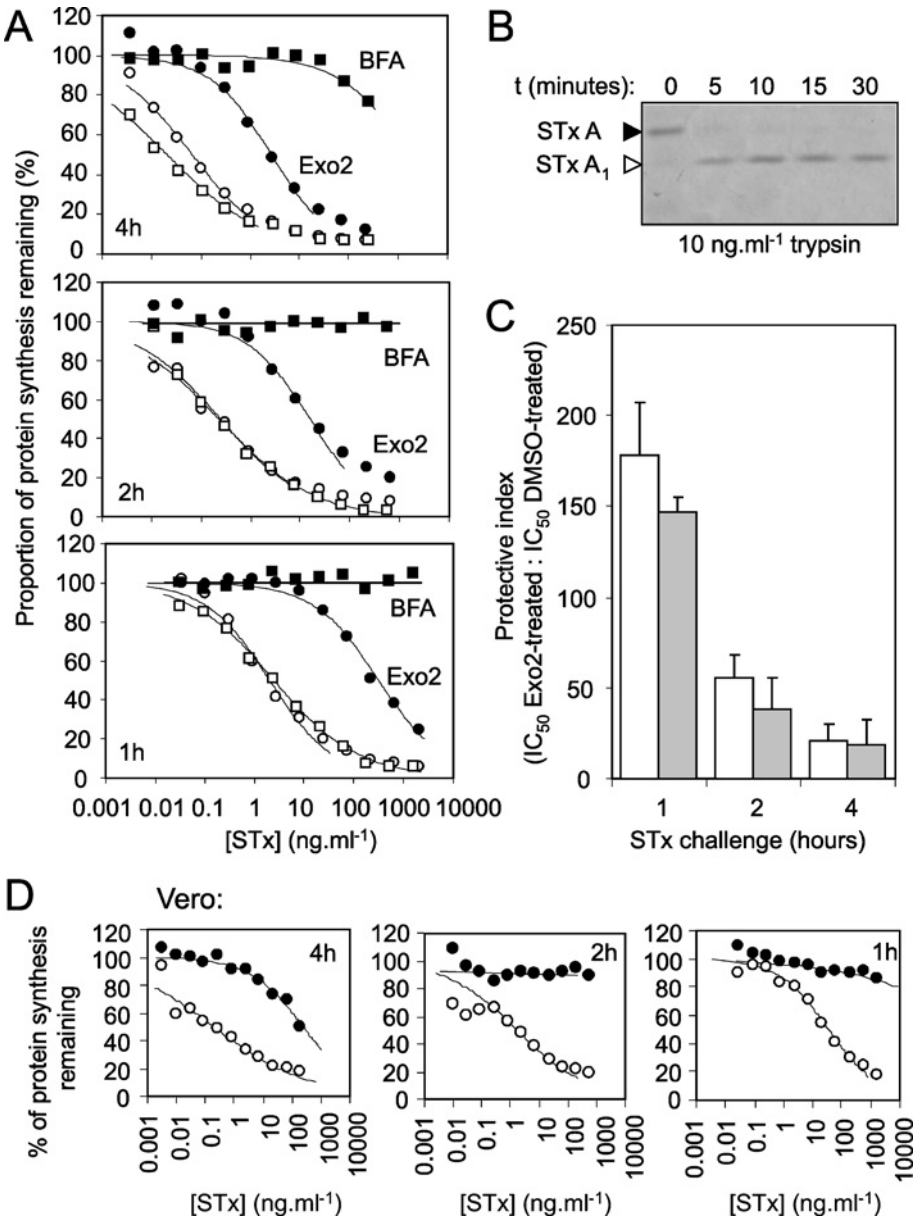

Figure 2 Exo2 treatment protects HeLa and Vero cells against STx challenge

(**A**) HeLa cells pre-treated with DMSO, DMSO/Exo2, ethanol vehicle (ethanol) or ethanol/BFA for 30 min at 37 °C were treated with graded doses (20 μg · ml^{-1} to 0.05 ng · ml^{-1}) of STx in medium containing DMSO, DMSO/Exo2, ethanol, or ethanol/BFA as appropriate for 4 h (top panel), 2 h (middle panel) or 1 h (bottom panel), and their ability to synthesize proteins was subsequently determined. Typical single assays are shown. ○, DMSO-treated; ●, DMSO/Exo2-treated; □, ethanol-treated; ■, ethanol/BFA-treated. (**B**) STx was treated with trypsin (10 ng · ml^{-1}) for various lengths of timeas indicated (min) at 37 °C, and the STx A chain (black arrowhead) and nicked STx A1 chain (white arrowhead) products were separated by reducing-gel electrophoresis and revealed by Coomassie Brilliant Blue staining. (**C**) DMSO- and DMSO/Exo2-pre-treated cells were challenged with graded doses of non-nicked (white bars) or pre-nicked (grey bars) STx as in (**A**) for the times indicated (1, 2 or 4 h) at 37 °C after treatment with 10 ng · ml^{-1} trypsin for 30 min at 37 °C in medium containing DMSO or DMSO/Exo2 as appropriate, and the sensitivities to toxin (IC_{50}) were determined. The protective index is the ratio of IC_{50} Exo2-treated cells/IC_{50} control DMSO-treated cells. Results are means ± S.D. ($n = 3$) (**D**) Vero cells pre-treated with DMSO or DMSO/Exo2 for 30 min at 37 °C were treated with graded doses of STx in medium containing DMSO or DMSO/Exo2 as appropriate for the times indicated (1, 2 and 4 h) at 37 °C, and their ability to synthesize proteins subsequently was determined. Typical single assays are shown. ○, DMSO-treated; ●, DMSO/Exo2-treated.

(Figure 2D), and too large to measure at the concentrations of toxin used here for 2 h and 1 h challenges. In contrast, BS-C-1 cells were resistant to STx challenge at the times and concentrations of toxin used here (results not shown). This was most likely the result of an absence of functional Gb3 receptors. Indeed, in human intestinal T84 cells, in which there is no detectable effect on the time course of CTx action [18], it is known that only ~5 % of cells express the STx receptor [35]. Accordingly, T84 cells were found to be resistant to STx under the conditions of toxin challenge used here (results not shown). Furthermore, butyric acid treatment, which is known to sensitize some resistant cell lines to STx by inducing synthesis of productive receptors [36,37], was also ineffective when used on BS-C-1 and T84 cells (results not shown). Thus neither BS-C-1 nor T84 cells can be used to test the effect of Exo2 on the retrograde trafficking of STx.

We conclude that Exo2 treatment severely impairs, but does not completely inhibit, the trafficking of STx to the ER in STx-sensitive cells, even though it has no effect on CTx when tested

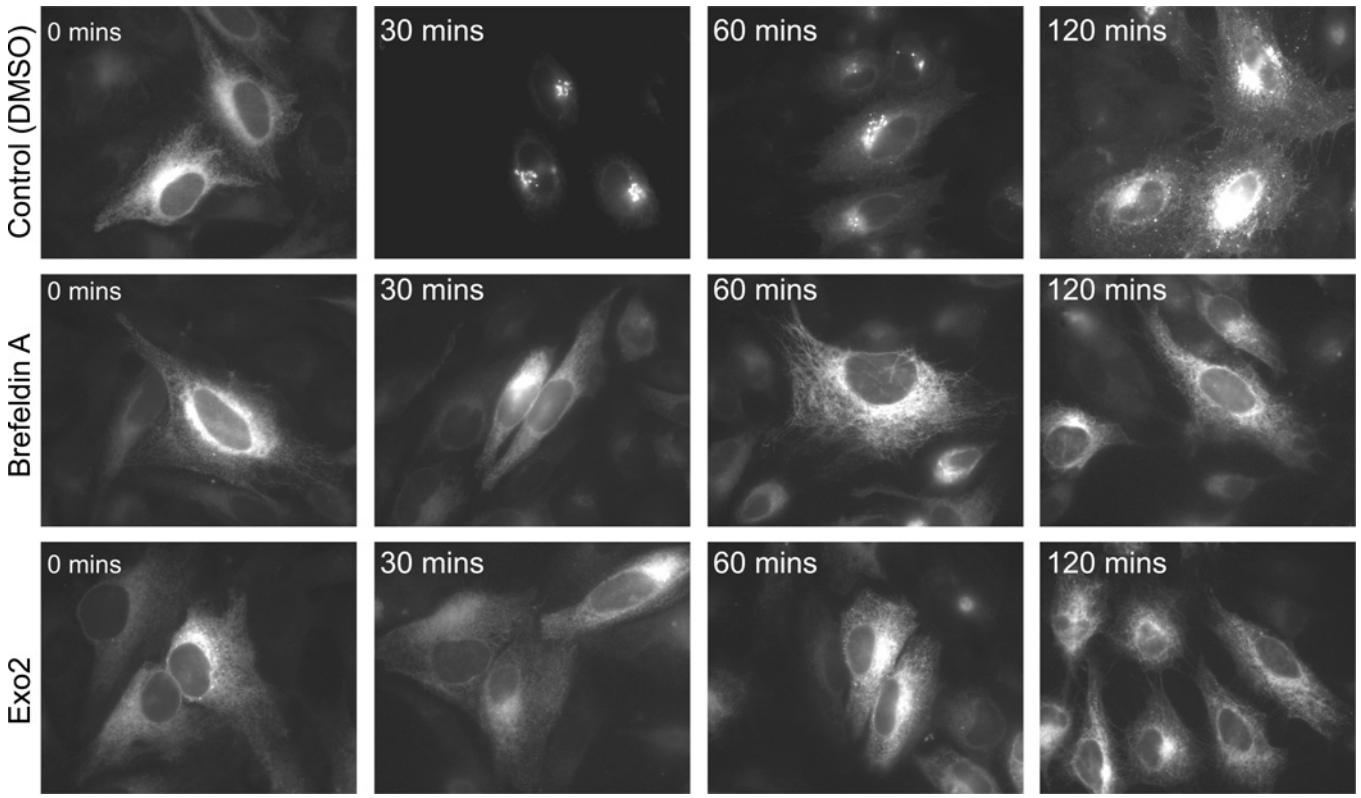

Figure 3 Exo2 inhibits secretory transport of tsO45-G–YFP

HeLa cells were transfected with a plasmid encoding tsO45-G–YFP and incubated at 39.5 °C for 16 h to accumulate the protein in the ER. Cells were subsequently incubated at 39 °C for a further 2 h in the presence of DMSO (Control), 10 μg · ml^{-1} BFA or 50 μM Exo2. Cells were then temperature-shifted to 32 °C to allow export of tsO45-G–YFP from the ER for the times indicated (0, 30, 60 and 120 min).

in these cells [18], and that the magnitude of the protective effect varies with cell type.

Exo2 disperses the TGN in HeLa cells

The changing cytotoxicity profile seen with time in STx-sensitive cells might indicate an incomplete effect of Exo2, such that after longer toxin exposures (4 h), sufficient STx was able to reach the ER to enter the cytosol and inhibit protein synthesis. Alternatively, it may point to a gradual functional recovery of the toxin entry pathway. To examine this further, we analysed the effects of Exo2 on secretion and the gross morphology of organelles known to be required for normal STx retrograde trafficking. We initially performed these experiments in HeLa cells, where the changing profile of the effects of Exo2 with time of exposure is most readily measured (Figure 2).

As expected, Exo2 acted as a secretion inhibitor, blocking the ER-to-Golgi export of tsO45-G (temperature-sensitive vesicular-stomatitis virus-G mutant)–YFP (yellow fluorescent protein), a classic marker for secretory protein transport [38,39]. In control cells, tsO45-G–YFP was released from the ER to the Golgi and the cell surface after a temperature shift from 39.5 °C to 32 °C (Figure 3). In contrast, in cells incubated with either 50 μM Exo2 or 10 μg · ml^{-1} BFA, tsO45-G–YFP remained within the ER compartment following the temperature shift, even in prolonged time-course experiments (results not shown). These effects are indistinguishable from those reported previously in Exo2-treated BS-C-1 cells [18].

We then examined the effects of a 2 h Exo2 treatment on the gross morphology of intracellular compartments using indirect immunofluorescence (Figure 4). Since Exo2 blocks secretory cargo export from the ER, the distribution of COPII (coatomer protein II) coat proteins was examined using antibodies raised against the Sec31A (Figure 4) and Sec24C components (results not shown). Their location and the rate of their recycling on and off the ER membrane (measured using EGFP–Sec24C or EGFP–Sec31A) remained unchanged following Exo2 treatment (results not shown). EEs (labelled using EEA1) also showed no change in gross morphology or distribution (Figure 4). However, Exo2 treatment did stimulate a redistribution of giantin from the Golgi to the ER/ERGIC, although ERGIC-53 itself was relocated to the ER and COPI was released from the Golgi and ERGIC membranes to a cytosolic location. These effects of Exo2 are consistent with the disruption of the COPI-dependent pathway and Golgi apparatus as observed previously [18]. Unexpectedly, and in contrast with a previous report [18], the TGN marker golgin-97 redistributed from a classic juxtanuclear position to a peripheral localization in the presence of Exo2 (Figure 4). These results suggest that, in HeLa cells, Exo2 may have very similar effects on the Golgi and the TGN as BFA. This was examined in more detail using time-lapse microscopy.

First, we followed the distribution of a EGFP-tagged marker of the Golgi apparatus, NAGFP (EGFP fused to the Golgi retention signal of *N*-acetylglucosaminyltransferase I) [40]. As expected, BFA caused a complete and rapid redistribution of NAGFP to the ER (Figure 5A and Supplementary Movie S1 at http://www.

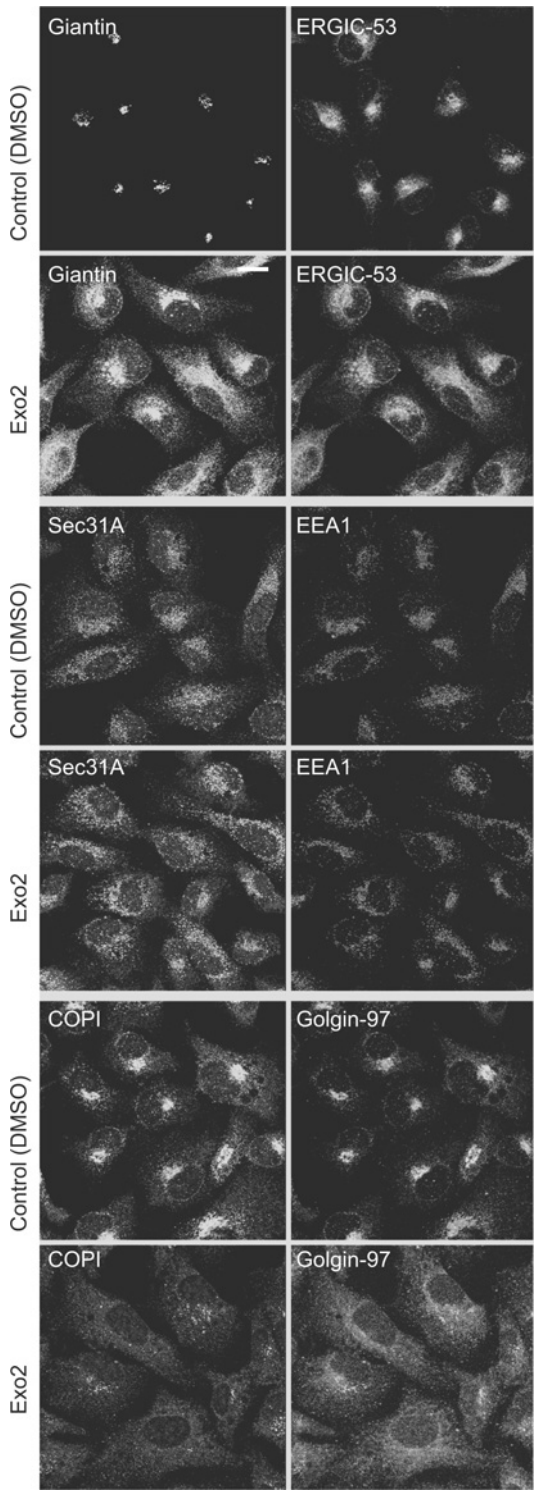

Figure 4 Steady-state localization of endomembranes is perturbed by Exo2

HeLa cells were incubated with 50 μM Exo2 for 2 h at 37 °C, followed by fixing and processing for immunofluorescence with antibodies specific for the proteins indicated. Cells were then imaged using confocal microscopy; images shown represent maximum intensity projections of ten *z* slices through each sample. Control is untreated cells incubated with DMSO.

BiochemJ.org/bj/414/bj4140471add.htm). A similar rapid redistribution occurred in ~90 % of Exo2-treated cells. Secondly, given the discrepancy between our observations of an Exo2-mediated disruption of the TGN, as visualized through a redistribution of golgin-97, and a published report showing that Exo2 has no effect on the TGN marker TGN46 in monkey BS-C-1 cells [18], we examined the location of these two proteins in time-course experiments. In HeLa cells, Exo2 promoted a redistribution of TGN46 and golgin-97 from a juxtanuclear location to a peripheral pattern within 60 min (Figures 5B and 5C). Interestingly, at later time points (e.g. 300 min), we consistently observed a sub-population of cells in which the original juxtanuclear localization became more prominent (Figures 5B and 5C, arrows). After a 1 h incubation with Exo2, 90 % of cells showed disrupted TGN46 localization (Figure 6). These results are consistent with the known effects of BFA on TGN morphology where the redistribution of TGN markers is also non-uniform [7,8,41].

Next, we compared the effects of Exo2 in HeLa and BS-C-1 cells (see Supplementary Figure S1 at http://www.BiochemJ.org/bj/414/bj4140471add.htm). We found that in BS-C-1 cells the TGN becomes dispersed, but a remnant remains at the classical juxtanuclear position following Exo2 treatment. This indicates a partial but incomplete dispersion of the TGN in BS-C-1 cells treated with Exo2 and clarifies the difference between our results and the results published previously [18]. We then investigated whether or not Exo2 treatment stimulates TGN–endosome fusion in HeLa cells (see Supplementary Figure S2 at http://www.BiochemJ.org/bj/414/bj4140471add.htm). TGN46 redistributed after Exo2 treatment to structures localized near EEs. No fusion was seen with these structures, late endosomes (stained with CD63) nor lysosomes (labelled with LysoTracker). No plasma-membrane co-localization was seen (results not shown).

Thus in both HeLa and BS-C-1 cells, the effects of Exo2 on ERGIC and Golgi membranes are very similar to those of BFA, but with respect to the TGN, there is a highly significant difference: whereas BFA induces tubulation of the TGN [7], Exo2 does not. The TGN is nevertheless dispersed by Exo2 in both cell types, although there are cell-type-specific differences in the magnitude of this response. In a fraction of the Exo2-treated HeLa cells, the TGN staining pattern that was lost at early time points became partly restored with increasing lengths of Exo2 incubation, which may point to a recovery of the TGN over time. Thus the changing STx cytotoxicity profile with time (Figure 2) might be explained by a partial recovery of functional organelles.

Exo2 retards the ER delivery of STx in HeLa cells

Retrograde trafficking of STx can be monitored using a recombinant STxBsulf cargo containing an accessible sulfation site that permits *in vivo* modification by the addition of $^{35}SO_4^{2-}$ in a reaction catalysed by TPST [22,42]. In Exo2-treated cells, we observed retarded kinetics of STxB sulfation following both 20 min treatment with STxBsulf (Figure 7A) and in a time course of toxin treatment (Figure 7B). The overall level of protein sulfation was reduced in Exo2-treated cells. Normalization of results to total sulfation counts for each time point revealed a delay of at least 60 min in reaching the sulfation compartment following Exo2 treatment, with the peak of sulfation occurring between 2–4 h in Exo2-treated cells compared with just 1 h in control cells (Figure 7C). Thus Exo2 treatment causes a delay in the arrival of STxB to the sulfation compartment.

The site of this modification in mammalian cells has been variously reported to be the *trans*-Golgi compartment (i.e. part of the cisternal stack) or the TGN, which is directly apposed to the *trans*-Golgi itself [22,43,44]. Since the sulfation assay defines the arrival of cargo at a TPST-containing compartment, we examined the cellular site of the two human TPST1 and TPST2 isoforms [45,46] in the presence and absence of Exo2. As available

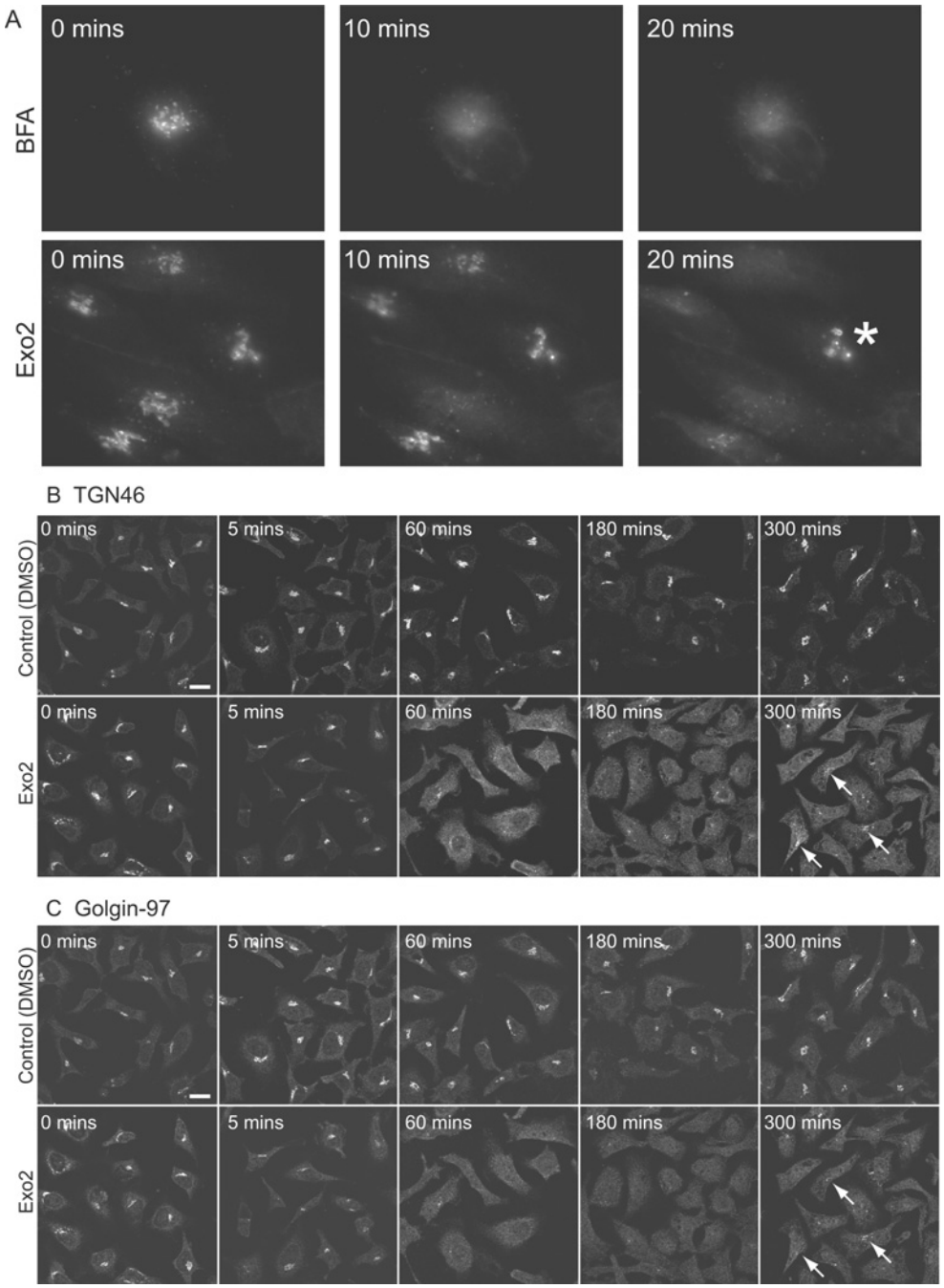

Figure 5 Perturbation of Golgi and TGN markers by Exo2

(**A**) HeLa cells transfected with NAGFP were incubated in the presence of either BFA (upper panels) or 50 μM Exo2 (lower panels) at 37 °C and imaged using time-lapse microscopy immediately after the addition of inhibitors. Still images at 0, 10, or 20 min after the addition of inhibitors are shown. The asterisk (*) marks a Golgi apparatus that is relatively Exo2-resistant. (**B** and **C**) Cells were incubated with either DMSO or 50 μM Exo2 at 37 °C and fixed after incubation for various time points (0, 5, 60, 180 and 300 min) and processed for immunofluorescence using antibodies directed against TGN46 (**B**) or golgin-97 (**C**). Note that the panels in (**B**) and (**C**) are from the same cells, double-labelled for these markers. Arrows indicate re-emergence of juxtanuclear staining.

antibodies were not effective for *in vivo* immunolabelling (results not shown), we generated C-terminal EGFP-tagged versions for expression and imaging. TPST1/2 are type I integral membrane proteins, and so C-terminal tagging circumvents any potential problems of the tag interfering with the N-terminal signal sequence.

Transient expression of either TPST1–EGFP or TPST2–EGFP at low levels in HeLa cells resulted in their localization to a juxtanuclear pool consistent with either Golgi or TGN membranes (Figure 8A), with a small amount in peripheral punctae. Following incubation with BFA or Exo2, the bulk of TPST1–EGFP and TPST2–EGFP was seen to relocate to the ER, although some peripheral punctate labelling remained (Figure 8A). Subsequent results are shown for TPST1–EGFP, but indistinguishable results were seen using TPST2–EGFP (results not shown). In the presence of Exo2, the majority of TPST1–EGFP co-localized with

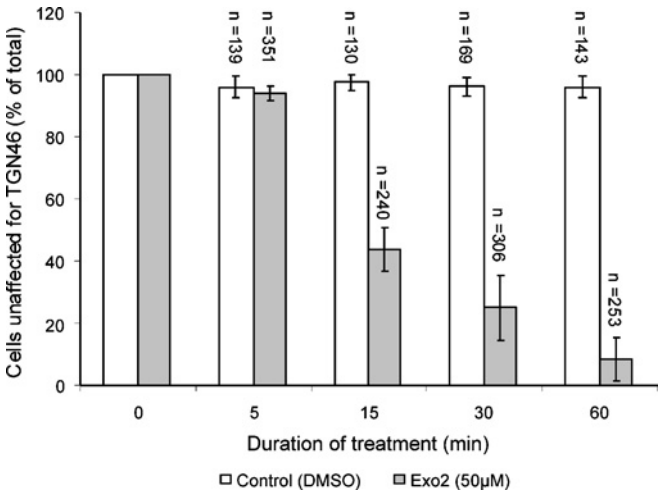

Figure 6 Quantification of organelle disruption by Exo2

Cells processed as in Figure 4 were quantified for TGN46 localization. The histogram shows the percentage of cells with disrupted TGN46 localization at the indicated time points after addition of DMSO (white bars) or Exo2 (grey bars). Results are means ± S.D.

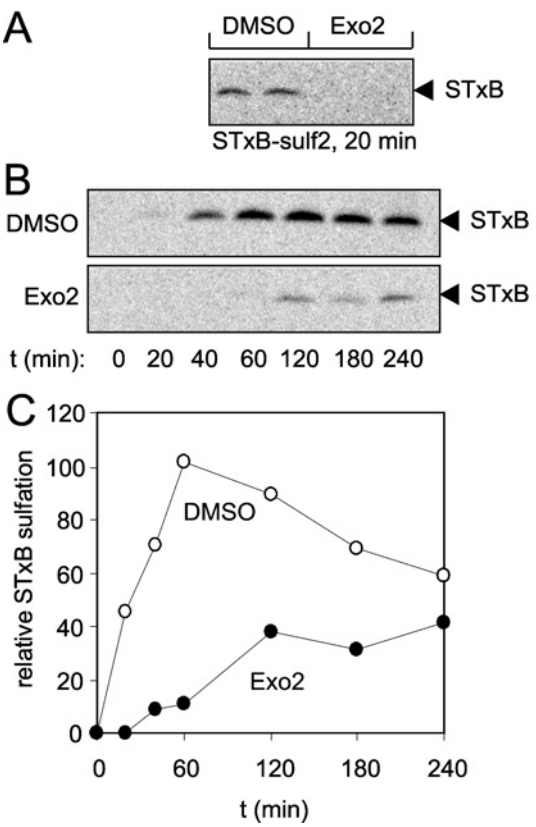

Figure 7 Exo2 treatment retards the sulfation of STxB chain

(**A**) Treatment of HeLa cells with Exo2 prevents sulfation of STxBsulf (arrowhead) 20 min post-internalization. Cells were pre-treated with 50 μM Exo2 for 30 min at 37 °C, incubated with STxB on ice and then further incubated for 20 min in the presence of Exo2 (see the Experimental section).(**B**) Time courses of STxB sulfation (arrowhead). Upper panel: during DMSO treatment; lower panel: during Exo2 treatment. Cells were pre-treated with 50 μM Exo2 for 30 min at 37 °C, incubated with STxB on ice and then further incubated for 0, 20, 40, 60, 120, 180 and 240 min in the presence of Exo2 (see the Experimental section). (**C**) Relative STxB sulfation profiles after DMSO (○) and Exo2 treatment (●; 50 μM Exo2), normalized to general sulfation levels.

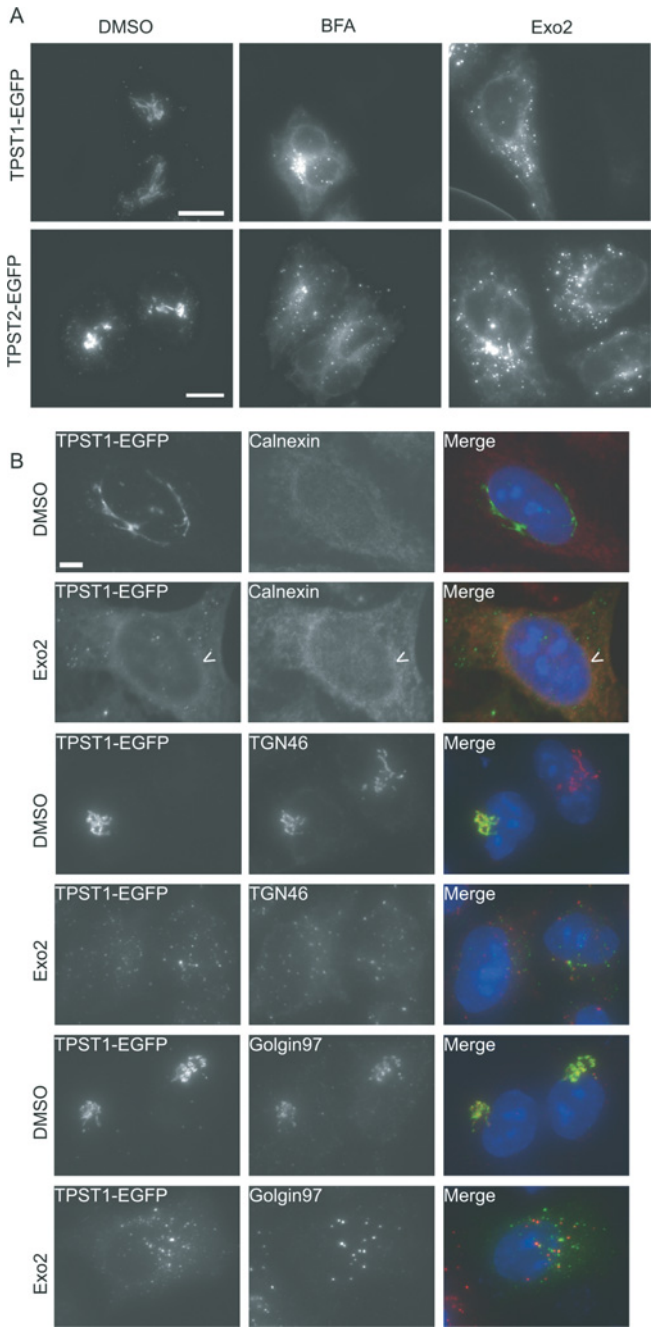

Figure 8 TPST1–EGFP predominantly localizes to the trans-Golgi

(**A**) TPST1–EGFP or TPST2–EGFP transiently expressed in HeLa cells at low levels of expression were imaged after treatment in the absence or presence of DMSO, BFA and 50 μM Exo2 for 2 h at 37 °C as indicated. Scale bar, 20 μm. (**B**) HeLa cells transiently expressing TPST1–EGFP were treated for 1 h at 37 °C with DMSO or 50 μM Exo2 diluted in culture medium, fixed and immunolabelled using the indicated antibodies. Typically, 10 stacks were acquired through the sample. For calnexin labelling, a single *z* slice is shown and the arrowhead points to the nuclear envelope. Other images shown represent the maximum projection of the *z* stacks. Indistinguishable results were obtained for TPST2–EGFP (results not shown). Scale bar, 5 μm.

calnexin, a marker of the ER; some peripheral punctate localization remained, but this pool of TPST1–EGFP did not co-localize with any marker tested, including TGN46 and golgin-97 (Figure 8B). Double-labelling experiments revealed that, at steady-state, TPST1–EGFP partially overlaps with both GalT, a *cis-medial* Golgi marker, and TGN46, a definitive marker for the

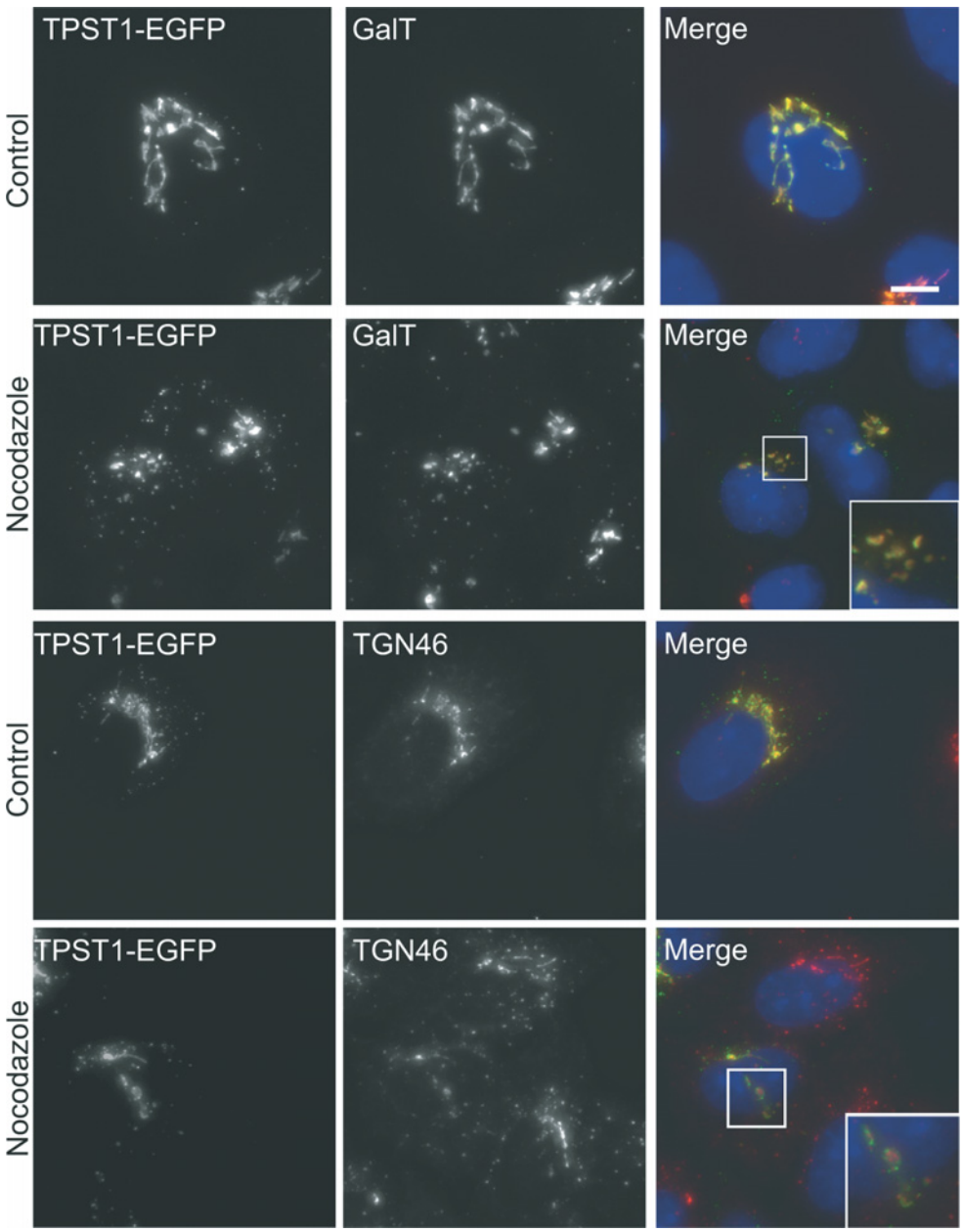

Figure 9 TPST1–EGFP co-localizes with GalT in nocodazole-induced mini Golgi stacks

TPST1–EGFP was expressed in HeLa cells which, where indicated, were incubated in the presence of nocodazole before fixing and immunolabelling for the Golgi marker GalT or the TGN marker TGN46 as indicated. Indistinguishable results were obtained using TPST2–EGFP (results not shown). Scale bar, 20 μm. Insets show 2 $\times$ enlargements of the boxed regions. Note the absence of co-localization with TGN46.

TGN [47,48] (Figure 9). To examine this in more detail, cells were treated with nocodazole to depolymerize microtubules and scatter the Golgi apparatus; scattered Golgi elements in this experiment retain their *cis–trans* polarity [49]. These Golgi elements showed a clear distinction between the localization of TPST1–EGFP and TGN46, with a higher degree of co-localization seen between GalT and TPST1–EGFP (Figure 9) and golgin-97 (results not shown). Similar results were obtained by co-staining for GM130 and TPST-1 (results not shown). The identity of the peripheral punctae is not known, although some but not all co-localize with GalT, indicating they are scattered Golgi elements. Although these punctae were positive for TPST1–EGFP in BFA-treated cells, they were shown not to stain for EEA1, CD63 or ERGIC-53, indicating that they do not represent early- or late-endosomal membranes or the ERGIC compartment respectively (results not shown). Exo2 did not induce tubulation of the TGN in these cells, nor in live cells expressing low levels of TPST–EGFP (results not shown).

Together these results indicate that in HeLa cells, the majority of TPST is normally localized in the GalT-containing *trans*-Golgi cisternae, and that upon Exo2 treatment, TPST is relocalized to the ER. Thus the most rational explanation for the kinetic delay in sulfation of STxBsulf (Figure 7) is that the sulfation assay measures the delivery of STxB from the dispersed TGN and/or endosomes to the ER.

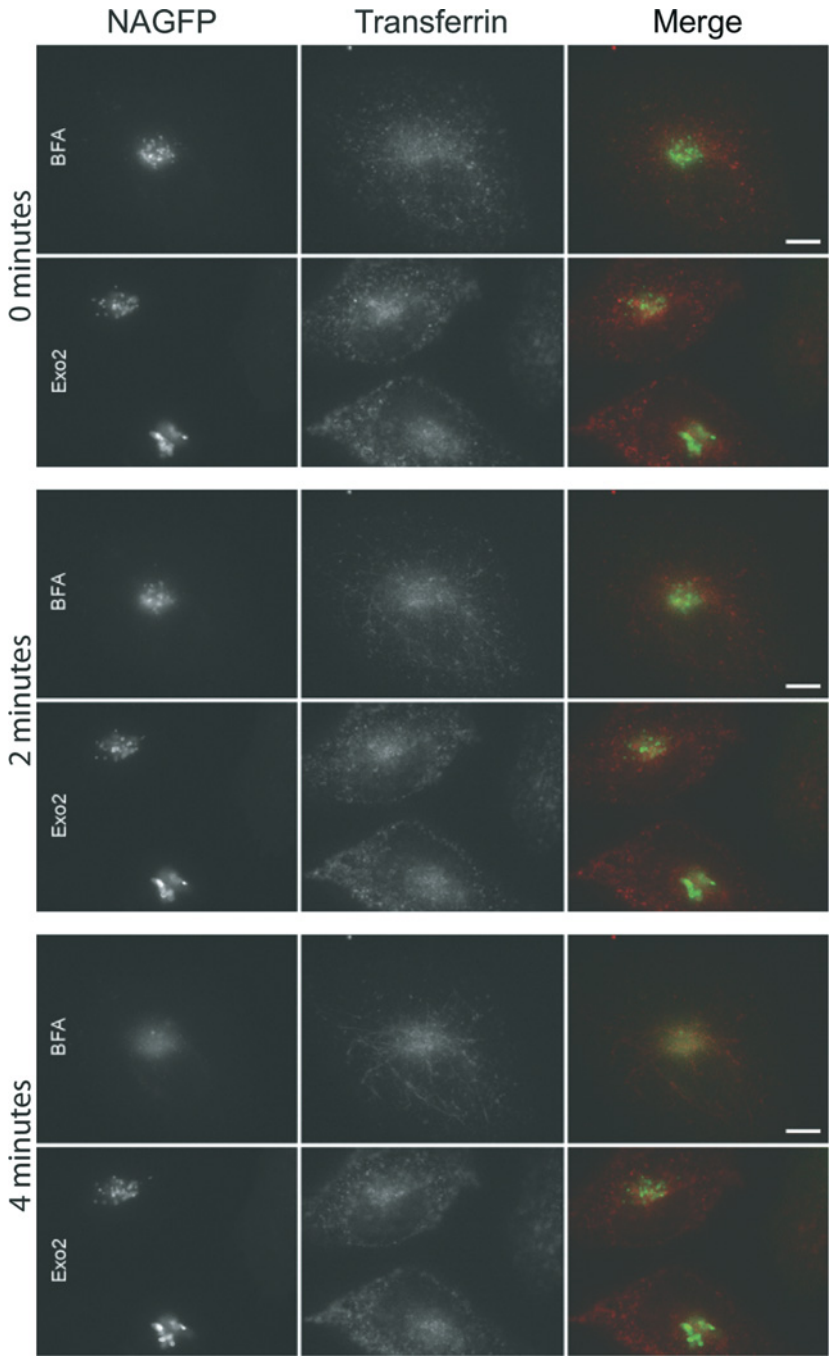

Figure 10 BFA, but not Exo2, induces tubulation of early endocytic compartments

Cells loaded with fluorescent transferrin for 5 min at 37 °C were imaged by time-lapse microscopy in the presence of either BFA (top panels) or 50 μM Exo2 (lower panels). The time-lapse sequence is included as Supplementary Movie S1 (see http://www.BiochemJ.org/bj/414/bj4140471add.htm), and still images taken at 0, 2 and 4 min after addition of BFA or Exo2 are shown. Note the extensive tubulation of EEs following the addition of BFA, which are never observed following the addition of Exo2. Scale bar, 20 μm.

Exo2 blocks delivery of STx to the disrupted TGN of HeLa cells

Next, we examined the effect of Exo2 on the early-endosomal compartment, through which STx normally traffics en route to the TGN. A well-characterized effect of BFA is its ability to cause the tubulation of EEs [7,8]. To test the effects of Exo2 on EE tubulation, cells were loaded with fluorescent transferrin for 5 min, before adding DMSO, BFA or Exo2, and then imaged immediately. Figure 10 reveals that untreated cells show a classic distribution of transferrin in small punctae throughout the cell (0 min time point). On addition of DMSO, these punctae do not appear to change (results not shown). However, on addition of BFA, the expected extensive tubulation of this EE compartment (2 and 4 min time points) was observed [7]. In stark contrast, Exo2 did not result in tubulation of endosomes, and cells appeared to be indistinguishable from controls (Figures 4 and 10, bottom panels). Time-lapse data from the experiments shown in Figure 10 are included in Supplementary Movie S1 (at http://www.

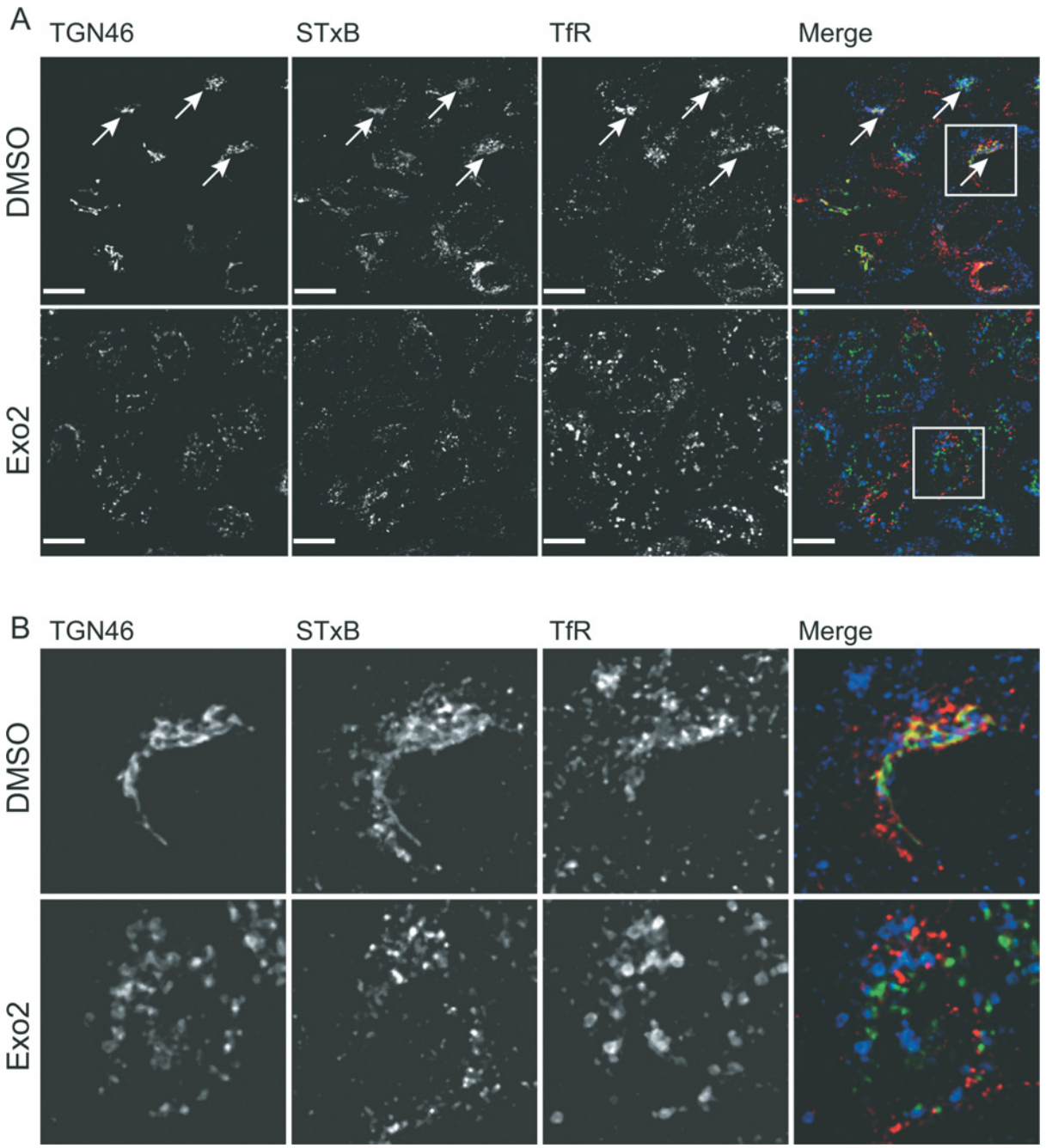

Figure 11 Exo2 inhibits transit of STxB to the TGN

(**A**) HeLa cells were pre-treated with 50 μM Exo2 for 30 min at 37 °C, stained with Cy3-labelled STxB (red) on ice followed by warming to 37 °C for 90 min in the presence of Exo2. Cells were fixed and immunolabelled with antibodies against TGN46 (green) and the TfR (blue). Extensive co-localization of TGN46 and STxB is seen in control cells (arrows), but not in Exo2-treated samples. STxB also did not co-localize with TGN46 at either 45 min or 120 min at 37 °C (results not shown) in Exo2-treated cells. TfR labelling is also seen in close proximity to that of STxB and TGN46 in controls, but not in Exo2-treated cells. Images shown are maximum intensity projections of 10 confocal *z* slices (pinhole at 1 Airy unit) that have been processed in Volocity 4.3 (Improvision) with a low-pass noise filter. Scale bar, 10 μm. (**B**) Enlargements ($\times$ 4) of the boxed regions.

BiochemJ.org/bj/414/bj4140471add.htm). In order to confirm the efficacy of Exo2 in these experiments, cells were transfected with a plasmid expressing NAGFP [40] prior to loading with transferrin. This enabled us to confirm that the Golgi structure was disrupted, despite there being no tubulation of transferrin-positive EEs in the same cells (results not shown). Thus while the effects of Exo2 on ERGIC and Golgi membranes are very similar to those of BFA in HeLa cells (see above), there are striking differences in their effects on the TGN and EEs. Even after lengthy incubations (2 h) with high concentrations of Exo2, we could detect no endosomal tubulation (results not shown).

We then examined the arrival of toxin to the TGN following its application at the cell surface (Figure 11). Since TPSTs are redistributed to the ER by Exo2 treatment, they cannot be regarded as a reliable marker of TGN arrival in Exo2-treated cells. We therefore monitored the transport of Cy3-labelled STxB into TGN46-positive compartments. In control cells, 90 min after exposure to STxB, immunofluorescence labelling showed

extensive co-localization with TGN46 (Figure 11). At the same time, in Exo2-treated cells, no significant co-localization with TGN46 was noted. This suggests that the primary block in retrograde transport of STx induced by Exo2 treatment lies between an endosomal compartment and the TGN, with perhaps a further block between the TGN and the Golgi caused by collapse of the Golgi stack into the ER. Thus at all the time points tested following Exo2 treatment, STxB-labelled endosomes and the TGN remain as distinct organelles; we also note that STxB and transferrin labelling remains distinct following Exo2 incubation, indicating that STxB and transferrin either label distinct domains of the same endosome or, more likely, they label distinct endosomes. We also note that the juxtanuclear clustering of the TfR in control cells is perturbed following incubation with Exo2. This hints at the possible perturbation of centripetal movement of EEs in Exo2-treated cells, possibly through inhibition of minus-end-directed microtubule-based transport.

DISCUSSION

Our results show that Exo2 has overlapping but distinct effects on membrane trafficking in mammalian cells compared with the widely used compound BFA. BFA and Exo2 appear indistinguishable in terms of disrupting anterograde traffic from the ER to the Golgi and in perturbing the juxtanuclear localization of the Golgi stack. In contrast with a report published previously [18], we also find that when the widely used HeLa epithelial cell line is treated with Exo2, it causes dispersion of the TGN, like BFA. We note that there are cell-type differences in the severity of the Exo2-induced effect, with a less pronounced effect on the TGN in BS-C-1 cells. However, Exo2 does not cause the tubulation that has been observed for some TGN markers when cells are treated with BFA [7]; it does not induce tubulation of endosomes, even after prolonged treatment, and it does not impede the uptake of STx into endosomes. The major difference in cellular morphological changes stimulated by the two reagents appears to be that although BFA disrupts the cell at the level of the ER/Golgi and the endosome/TGN interfaces, the major effects of Exo2 appear largely to be restricted to the TGN, Golgi stack and the ER. Upon closer examination, we find that Exo2 treatment has subtle effects at the endosomal level, inhibiting the transfer of internalized STxB to the TGN.

The morphological description of the Exo2 phenotype that we provide is complemented by inspection of the retrograde-uptake pathway of STx and STxB, its cell-binding B chain. These proteins provide useful probes to test the functionality of retrograde transport routes, since they normally traffic via the EEs, TGN and Golgi to the ER [22,25,50], where the A chain of the holotoxin retrotranslocates across the ER membrane to damage target ribosomes. Thus inhibition of protein synthesis can be used to monitor successful negotiation of the retrograde-transport pathway, and sulfation can be used to measure the arrival of STxB in the sulfation compartment. In this way, the sulfation of a modified CTx and the activation of its cytosolic target, adenylyl cyclase, in Exo2-treated epithelial cells in which the integrity of the TGN was retained, led to the proposal of a direct and efficient TGN-to-ER lipid-dependent sorting pathway [18]. CTx and STx bind cell-surface ganglioside GM1 and Gb3 respectively, and normally traffic via EEs and the TGN to the ER lumen in association with detergent-resistant lipid microdomains, in a manner that is not dependent on either KDEL receptors or COP1 transport intermediates [23–26]. Although much is known about their intracellular trafficking, it remains unclear whether the lipid-transport pathway is utilized only by ganglioside-binding proteins or whether it is also exploited by proteins that interact with other microdomain-enriched lipids. We therefore tested the effects of Exo2 on the uptake of STx. Since Exo2 did not disrupt the lipid-dependent sorting pathway believed to be used by proteins such as STx and CTx [18], it was anticipated that the entry of STx would be unaffected.

Unexpectedly, the present paper reveals that the transport of STx in HeLa cells is very severely hampered by Exo2 treatment, particularly following short (1–2 h) challenges with toxin. The magnitude of these effects after a 1 h toxin challenge ($\sim$150-fold) shows that less than 1 % of the toxin that reaches the cytosol in Exo2-untreated cells reaches the cytosol in Exo2-treated cells. This would indicate that even in the $\sim$10 % of Exo2-treated cells that retain unchanged Golgi and TGN markers (Figure 5), retrograde transport through these structures is highly compromised. However, toxicity is not completely abrogated (as it is with BFA), indicating that the Exo2 block is either incomplete, permitting some residual retrograde transport, or that a much less efficient transport pathway operates from other compartments in the absence of a Golgi stack. Either way, the effects of Exo2 on STx uptake are markedly different from the reported effects on CTx uptake [18].

The observed delay in STx sulfation reported in the present paper (Figure 7) is consistent with a blockade in transport between the endosomes and TGN. However, a little-cited pleiotropic effect of BFA is the complete inhibition of the Golgi uptake of the activated substrate of TPST, PAPS (adenosine 3′-phosphate 5′-phosphosulfate) [51] and a total abrogation of protein sulfation [52]. The fact that the TPSTs continue to act upon their substrates in the presence of Exo2, as shown in the present paper and elsewhere [18], may therefore reflect either their relocation to the ER membrane or the action of TPST in the fragmented TGN, although we cannot detect its presence in the TGN in the experiments described here (Figure 8). Either way, our results point to difficulties in transporting STx from endosomes in Exo2-treated cells. This led us to examine the endosome/TGN interface more closely (Figures 10 and 11). The results point to an unexpected divergence in toxin trafficking. Although CTx and STx are normally transported to the Golgi along pathways generally considered to be indistinguishable [53], Exo2 has brought to light some subtle differences in their routing. Although the Exo2-induced collapse of the Golgi stack into the ER does not affect the transport of CTx [18], which can presumably bypass this organelle altogether, Exo2 severely impedes the uptake of STx. This suggests that STx is largely constrained to a transport pathway through the Golgi. However, the subtle spatial rearrangement of the endosome system induced by Exo2 treatment, and the failure of STx to efficiently access TGN46-positive compartments in Exo2-treated cells, perhaps points to an earlier separation of the toxin-trafficking routes, with a block at the EEs/TGN interface operating for STx, but not for CTx. The major target of Exo2 may therefore be a molecule involved in both early-endosomal delivery to the TGN and TGN access to the Golgi stack, or may be related proteins operating at both of these sites. Clearly the identification of the target(s) of Exo2 is an important next step.

Results were generated as follows: Figure 1 (G.J.C.), Figure 2 (R.A.S.), Figures 3, 4, 5 and 6 (P.W. and D.C.S.), Figure 7 (R.A.S. and M.A.), Figures 8, 9, 11, S1 and S2 (F.B.) and Figure 10 (P.W.). The manuscript was prepared by R.A.S. and L.M.R. D.J.S., L.J., J.M.L. and L.M.R. contributed to the design and execution of the project and analysis of the results. We thank Professor George Banting (Department of Biochemistry, University of Bristol, Bristol, U.K.) for the gift of of TGN46–GFP and Dr Harry Mellor (Department of Biochemistry, University of Bristol, Bristol, U.K.) for the gift of the mouse monoclonal anti-CD63 antibody. We thank the Medical Research Council (MRC) for providing an Infrastructure Award to establish the University of Bristol Cell Imaging

Facility. This work was generously supported by research grants from the Biotechnology and Biological Sciences Research Council (BBSRC) (BB/E012450/1; to D.J.S., G.J.C., L.M.R. and J.M.L.), the Wellcome Trust (080566Z/06/Z; to L.M.R. and J.M.L.), NIH (5U01A1658969-02; to R.A.S., L.M.R. and J.M.L.) and a Non-Clinical Senior Fellowship from the Medical Research Council (G117/554; to D.J.S.).

REFERENCES

1 Bonifacino, J. S. and Glick, B. S. (2004) The mechanisms of vesicle budding and fusion. Cell **116**, 153–166

2 Schekman, R. and Novick, P. (2004) 23 genes, 23 years later. Cell **116**, S13–S15

3 Donaldson, J. G., Lippincott-Schwartz, J., Bloom, G. S., Kreis, T. E. and Klausner, R. D. (1990) Dissociation of a 110-kD peripheral membrane protein from the Golgi apparatus is an early event in brefeldin A action. J. Cell Biol. **111**, 2295–2306

4 Orci, L., Tagaya, M., Amherdt, M., Perrelet, A., Donaldson, J. G., Lippincott-Schwartz, J., Klausner, R. D. and Rothman, J. E. (1991) Brefeldin A, a drug that blocks secretion, prevents the assembly of non-clathrin-coated buds on Golgi cisternae. Cell **64**, 1183–1195

5 Lippincott-Schwartz, J., Yuan, L. C., Bonifacino, J. S. and Klausner, R. D. (1989) Rapid redistribution of Golgi proteins into the ER in cells treated with brefeldin A: evidence for membrane cycling from Golgi to ER. Cell **56**, 801–813

6 Scheel, J., Pepperkok, R., Lowe, M., Griffiths, G. and Kreis, T. E. (1997) Dissociation of coatomer from membranes is required for brefeldin A-induced transfer of Golgi enzymes to the endoplasmic reticulum. J. Cell Biol. **137**, 319–333

7 Lippincott-Schwartz, J., Yuan, L., Tipper, C., Amherdt, M., Orci, L. and Klausner, R. D. (1991) Brefeldin A's effects on endosomes, lysosomes, and the TGN suggest a general mechanism for regulating organelle structure and membrane traffic. Cell **67**, 601–616

8 Wood, S. A., Park, J. E. and Brown, W. J. (1991) Brefeldin A causes a microtubule-mediated fusion of the trans-Golgi network and early endosomes. Cell **67**, 591–600

9 Reaves, B. and Banting, G. (1992) Perturbation of the morphology of the trans-Golgi network following Brefeldin A treatment: redistribution of a TGN-specific integral membrane protein, TGN38. J. Cell Biol. **116**, 85–94

10 Helms, J. B. and Rothman, J. E. (1992) Inhibition by brefeldin A of a Golgi membrane enzyme that catalyses exchange of guanine nucleotide bound to ARF. Nature **360**, 352–354

11 Jones, H. D., Moss, J. and Vaughan, M. (2005) BIG1 and BIG2, brefeldin A-inhibited guanine nucleotide-exchange factors for ADP-ribosylation factors. Methods Enzymol. **404**, 174–184

12 Zeghouf, M., Guibert, B., Zeeh, J. C. and Cherfils, J. (2005) Arf, Sec7 and Brefeldin A: a model towards the therapeutic inhibition of guanine nucleotide-exchange factors. Biochem. Soc. Trans. **33**, 1265–1268

13 Robineau, S., Chabre, M. and Antonny, B. (2000) Binding site of brefeldin A at the interface between the small G protein ADP-ribosylation factor 1 (ARF1) and the nucleotide-exchange factor Sec7 domain. Proc. Natl. Acad. Sci. U.S.A. **97**, 9913–9918

14 Peyroche, A., Antonny, B., Robineau, S., Acker, J., Cherfils, J. and Jackson, C. L. (1999) Brefeldin A acts to stabilize an abortive ARF-GDP-Sec7 domain protein complex: involvement of specific residues of the Sec7 domain. Mol. Cell **3**, 275–285

15 Zeeh, J. C., Zeghouf, M., Grauffel, C., Guibert, B., Martin, E., Dejaegere, A. and Cherfils, J. (2006) Dual specificity of the interfacial inhibitor brefeldin a for arf proteins and sec7 domains. J. Biol. Chem. **281**, 11805–11814

16 Mossessova, E., Corpina, R. A. and Goldberg, J. (2003) Crystal structure of ARF1*Sec7 complexed with Brefeldin A and its implications for the guanine nucleotide exchange mechanism. Mol. Cell **12**, 1403–1411

17 Feng, Y., Yu, S., Lasell, T. K., Jadhav, A. P., Macia, E., Chardin, P., Melancon, P., Roth, M., Mitchison, T. and Kirchhausen, T. (2003) Exo1: a new chemical inhibitor of the exocytic pathway. Proc. Natl. Acad. Sci. U.S.A. **100**, 6469–6474

18 Feng, Y., Jadhav, A. P., Rodighiero, C., Fujinaga, Y., Kirchhausen, T. and Lencer, W. I. (2004) Retrograde transport of cholera toxin from the plasma membrane to the endoplasmic reticulum requires the trans-Golgi network but not the Golgi apparatus in Exo2-treated cells. EMBO Rep. **5**, 596–601

19 Spooner, R. A., Watson, P. D., Marsden, C. J., Smith, D. C., Moore, K. A., Cook, J. P., Lord, J. M. and Roberts, L. M. (2004) Protein disulphide-isomerase reduces ricin to its A and B chains in the endoplasmic reticulum. Biochem. J. **383**, 285–293

20 Aghi, M., Kramm, C. M., Chou, T. C., Breakefield, X. O. and Chiocca, E. A. (1998) Synergistic anticancer effects of ganciclovir/thymidine kinase and 5-fluorocytosine/cytosine deaminase gene therapies. J. Natl. Cancer Inst. **90**, 370–380

20a Stephens, D. J. (2003) *De novo* formation, fusion and fission of COPII coated ER exit sites in mammalian cells. EMBO Rep. **4**, 210–217

21 Watson, P., Townley, A. K., Koka, P., Palmer, K. J. and Stephens, D. J. (2006) Sec16 defines endoplasmic reticulum exit sites and is required for secretory cargo export in mammalian cells. Traffic **7**, 1678–1687

22 Johannes, L., Tenza, D., Antony, C. and Goud, B. (1997) Retrograde transport of KDEL-bearing B-fragment of Shiga toxin. J. Biol. Chem. **272**, 19554–19561

23 Falguieres, T., Mallard, F., Baron, C., Hanau, D., Lingwood, C., Goud, B., Salamero, J. and Johannes, L. (2001) Targeting of Shiga toxin B-subunit to retrograde transport route in association with detergent-resistant membranes. Mol. Biol. Cell **12**, 2453–2468

24 Fujinaga, Y., Wolf, A. A., Rodighiero, C., Wheeler, H., Tsai, B., Allen, L., Jobling, M. G., Rapoport, T., Holmes, R. K. and Lencer, W. I. (2003) Gangliosides that associate with lipid rafts mediate transport of cholera and related toxins from the plasma membrane to endoplasmic reticulm. Mol. Biol. Cell **14**, 4783–4793

25 Girod, A., Storrie, B., Simpson, J. C., Johannes, L., Goud, B., Roberts, L. M., Lord, J. M., Nilsson, T. and Pepperkok, R. (1999) Evidence for a COP-I-independent transport route from the Golgi complex to the endoplasmic reticulum. Nat. Cell Biol. **1**, 423–430

26 Smith, D. C., Sillence, D. J., Falguieres, T., Jarvis, R. M., Johannes, L., Lord, J. M., Platt, F. M. and Roberts, L. M. (2006) The association of Shiga-like toxin with detergent-resistant membranes is modulated by glucosylceramide and is an essential requirement in the endoplasmic reticulum for a cytotoxic effect. Mol. Biol. Cell **17**, 1375–1387

27 Hallas, G. and Towns, A. D. (1996) A comparison of the properties of some 2-aminothiophene-derived disperse dyes. Dyes and Pigments **31**, 273–289

28 Joseph, P. S., Selladurai, S., Kanna, S. and Parthasarathi, V. (1990) Structure of 4-oxo-5,6,7,8-tetrahydro-3H-cyclohexathieno[2,3-d]pyrimidine. Acta Crystallogr. C **46**, 162–163

29 Ram, V. J., Pandey, H. K. and Vlietinck, A. J. (1981) Thieno[2,3-d]pyrimidines as potential chemotherapeutic agents. II. J. Heterocyclic Chem. **18**, 1277–1280

30 Shvedov, V. I., Ryzhkova, V. K. and Grinev, A. N. (1967) Synthesis of 4-hydroxythieno[2,3-d]pyrimidine derivatives. Khim. Geterotsikl. Soedin. **3**, 459–460

31 Ram, V. J. (1979) Thieno[2,3-d]pyrimidines as potential chemotherapeutic agents. Arch. Pharm. (Weinheim) **312**, 19–25

32 Robba, M. and Maume, D. (1972) Conditions of access to as-triazino(4,5-a)indole. Tetrahedron Lett. **13**, 2333–2335

33 Endo, Y., Tsurugi, K., Yutsudo, T., Takeda, Y., Ogasawara, T. and Igarashi, K. (1988) Site of action of a Vero toxin (VT2) from *Escherichia coli* O157:H7 and of Shiga toxin on eukaryotic ribosomes. RNA N-glycosidase activity of the toxins. Eur. J. Biochem. **171**, 45–50

34 Garred, O., van Deurs, B. and Sandvig, K. (1995) Furin-induced cleavage and activation of Shiga toxin. J. Biol. Chem. **270**, 10817–10821

35 Kovbasnjuk, O., Mourtazina, R., Baibakov, B., Wang, T., Elowsky, C., Choti, M. A., Kane, A. and Donowitz, M. (2005) The glycosphingolipid globotriaosylceramide in the metastatic transformation of colon cancer. Proc. Natl. Acad. Sci. U.S.A. **102**, 19087–19092

36 Sandvig, K., Ryd, M., Garred, O., Schweda, E., Holm, P. K. and van Deurs, B. (1994) Retrograde transport from the Golgi complex to the ER of both Shiga toxin and the nontoxic Shiga B-fragment is regulated by butyric acid and cAMP. J. Cell Biol. **126**, 53–64

37 Sandvig, K., Prydz, K., Ryd, M. and van Deurs, B. (1991) Endocytosis and intracellular transport of the glycolipid-binding ligand Shiga toxin in polarized MDCK cells. J. Cell Biol. **113**, 553–562

38 Gallione, C. J. and Rose, J. K. (1985) A single amino acid substitution in a hydrophobic domain causes temperature-sensitive cell-surface transport of a mutant viral glycoprotein. J. Virol. **54**, 374–382

39 Presley, J. F., Cole, N. B., Schroer, T. A., Hirschberg, K., Zaal, K. J. and Lippincott-Schwartz, J. (1997) ER-to-Golgi transport visualized in living cells. Nature **389**, 81–85

40 Shima, D. T., Haldar, K., Pepperkok, R., Watson, R. and Warren, G. (1997) Partitioning of the Golgi apparatus during mitosis in living HeLa cells. J. Cell Biol. **137**, 1211–1228

41 Reaves, B., Horn, M. and Banting, G. (1993) TGN38/41 recycles between the cell surface and the TGN: brefeldin A affects its rate of return to the TGN. Mol. Biol. Cell **4**, 93–105

42 Lee, R. W. and Huttner, W. B. (1983) Tyrosine-O-sulfated proteins of PC12 pheochromocytoma cells and their sulfation by a tyrosylprotein sulfotransferase. J. Biol. Chem. **258**, 11326–11334

43 Baeuerle, P. A. and Huttner, W. B. (1987) Tyrosine sulfation is a trans-Golgi-specific protein modification. J. Cell Biol. **105**, , 2655–2664

44 Huttner, W. B. (1988) Tyrosine sulfation and the secretory pathway. Annu. Rev. Physiol. **50**, 363–376
45 Beisswanger, R., Corbeil, D., Vannier, C., Thiele, C., Dohrmann, U., Kellner, R., Ashman, K., Niehrs, C. and Huttner, W. B. (1998) Existence of distinct tyrosylprotein sulfotransferase genes: molecular characterization of tyrosylprotein sulfotransferase-2. Proc. Natl. Acad. Sci. U.S.A. **95**, 11134–11139
46 Ouyang, Y., Lane, W. S. and Moore, K. L. (1998) Tyrosylprotein sulfotransferase: purification and molecular cloning of an enzyme that catalyzes tyrosine O-sulfation, a common posttranslational modification of eukaryotic proteins. Proc. Natl. Acad. Sci. U.S.A. **95**, 2896–2901
47 Ponnambalam, S., Girotti, M., Yaspo, M. L., Owen, C. E., Perry, A. C., Suganuma, T., Nilsson, T., Fried, M., Banting, G. and Warren, G. (1996) Primate homologues of rat TGN38: primary structure, expression and functional implications. J. Cell Sci. **109**, 675–685
48 Prescott, A. R., Lucocq, J. M., James, J., Lister, J. M. and Ponnambalam, S. (1997) Distinct compartmentalization of TGN46 and β1,4-galactosyltransferase in HeLa cells. Eur. J. Cell Biol. **72**, 238–246
49 Thyberg, J. and Moskalewski, S. (1985) Microtubules and the organization of the Golgi complex. Exp. Cell Res. **159**, 1–16
50 White, J., Johannes, L., Mallard, F., Girod, A., Grill, S., Reinsch, S., Keller, P., Tzschaschel, B., Echard, A., Goud, B. and Stelzer, E. H. (1999) Rab6 coordinates a novel Golgi to ER retrograde transport pathway in live cells. J. Cell. Biol. **147**, 743–760
51 Fjeldstad, K., Pedersen, M. E., Vuong, T. T., Kolset, S. O., Nordstrand, L. M. and Prydz, K. (2002) Sulfation in the Golgi lumen of Madin-Darby canine kidney cells is inhibited by brefeldin A and depends on a factor present in the cytoplasm and on Golgi membranes. J. Biol. Chem. **277**, 36272–36279
52 Muller, L., Barret, A., Picart, R. and Tougard, C. (1997) Proteolytic processing of sulfated secretogranin II in the trans-Golgi network of GH3B6 prolactin cells. J. Biol. Chem. **272**, 3669–3673
53 Nichols, B. J., Kenworthy, A. K., Polishchuk, R. S., Lodge, R., Roberts, T. H., Hirschberg, K., Phair, R. D. and Lippincott-Schwartz, J. (2001) Rapid cycling of lipid raft markers between the cell surface and Golgi complex. J. Cell Biol. **153**, 529–541

Received 18 January 2008/20 May 2008; accepted 4 June 2008
Published as BJ Immediate Publication 4 June 2008, doi:10.1042/BJ20080149

Biochem. J. (2008) **414**, 471–484 (Printed in Great Britain) doi:10.1042/BJ20080149

online data

SUPPLEMENTARY ONLINE DATA

The secretion inhibitor Exo2 perturbs trafficking of Shiga toxin between endosomes and the *trans*-Golgi network

Robert A. SPOONER*[1], Peter WATSON*[1,2], Daniel C. SMITH*[1,3], Frédéric BOAL†, Mohammed AMESSOU‡, Ludger JOHANNES‡, Guy J. CLARKSON§, J. Michael LORD*, David J. STEPHENS†[4] and Lynne M. ROBERTS*[4]

*Department of Biological Sciences, University of Warwick, Gibbet Hill Road, Coventry CV4 7AL, U.K., †Department of Biochemistry, University of Bristol, School of Medical Sciences, University Walk, Bristol BS8 1TD, U.K., ‡Institut Curie, Centre de Recherche, Laboratoire Trafic, Signalisation, et Ciblage Intracellulaires, 26 rue d'Ulm, 75248 Paris Cedex 05, France, and CNRS (Centre National de la Recherche Scientifique) UMR144, France, and §Department of Chemistry, University of Warwick, Gibbet Hill Road, Coventry CV4 7AL, U.K.

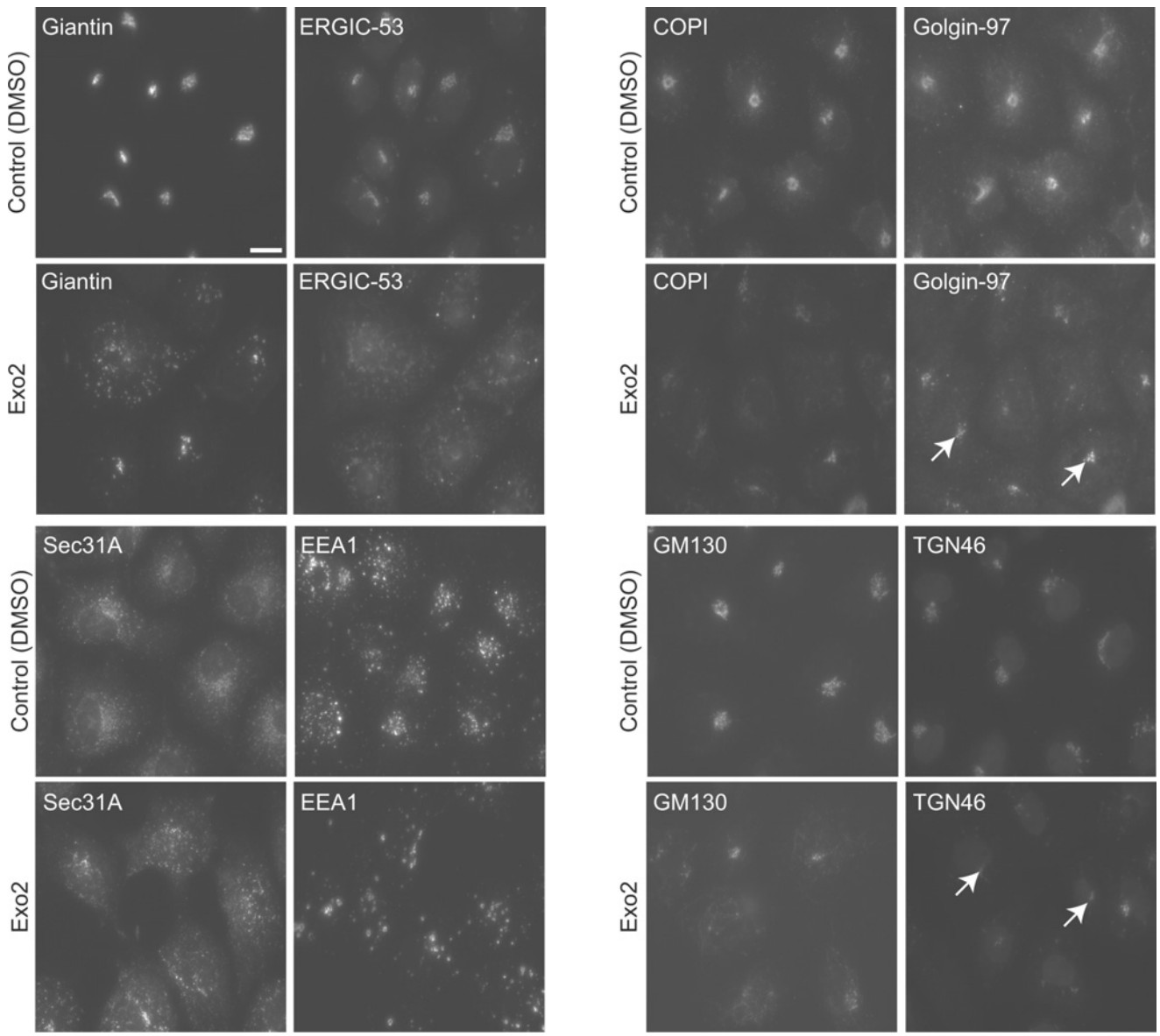

Figure S1 Effects of Exo2 on BS-C-1 cells

BS-C-1 cells (A.T.C.C. CCL-26) were treated with DMSO (Control) or with 50 μM Exo2 for 2 h at 37 °C, fixed, stained with the indicated antibodies and imaged on a wide-field microscope. The maximum intensity projection of at least ten *z* slices through the sample is shown. Arrows indicate examples of TGN remnants visible in BS-C-1 cells treated with Exo2 that retain their juxtanuclear position: TGN dispersion is less pronounced than in HeLa cells. Scale bar, 20 μm.

[1] These authors contributed equally to this work.
[2] Present address: School of Biosciences, Cardiff University, Museum Avenue, Cardiff CF10 3US, U.K.
[3] Present address: Cobra Biomanufacturing Plc, Stephenson Building, The Science Park, Keele ST5 5SP, U.K.
[4] Correspondence may be addressed to either of these authors (lynne.roberts@warwick.ac.uk or david.stephens@bristol.ac.uk).

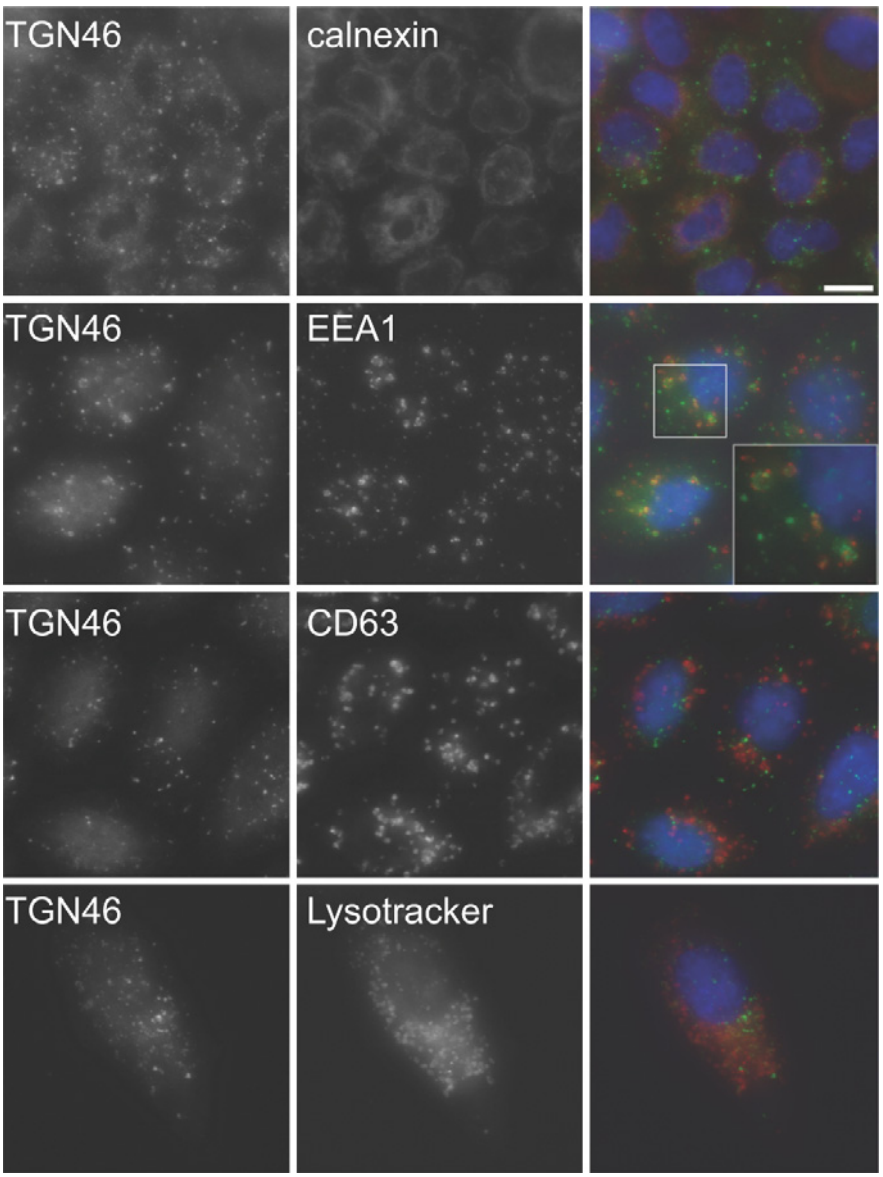

Figure S2 Localization of TGN46 in Exo2-treated cells

HeLa cells were treated with 50 μM Exo2 for 2 h at 37 °C, diluted in culture medium, fixed and processed for immunofluorescence with the indicated antibodies. Maximum projections of at least ten *z* stacks are shown. Exo2-induced altered TGN structures appeared to localize close to the EE (labelled by EEA1), but not to merge with the late endosomal (labelled with CD63) or lysosomal compartments (labelled by LysoTracker Red). Merge column (far right-hand side) shows DAPI (4′,6-diamidino-2-phenylindole; blue),TGN46 (green), and staining for calnexin, EEA1, CD63 and LysoTracker Red is shown in red as indicated. Scale bar, 10 μm.

Received 18 January 2008/20 May 2008; accepted 4 June 2008
Published as BJ Immediate Publication 4 June 2008, doi:10.1042/BJ20080149